



University of Kentucky
UKnowledge

Chemistry Faculty Publications

Chemistry

3-23-2015

Applied Quantum Chemistry: Spectroscopic Detection and Characterization of the F₂BS and Cl₂BS Free Radicals in the Gas Phase

Bing Jin

University of Kentucky, bing.jin@uky.edu

Phillip M. Sheridan

Canisius College

Dennis J. Clouthier

University of Kentucky, dclaser@uky.edu

Right click to open a feedback form in a new tab to let us know how this document benefits you.

Follow this and additional works at: https://uknowledge.uky.edu/chemistry_facpub

 Part of the [Chemistry Commons](#)

Repository Citation

Jin, Bing; Sheridan, Phillip M.; and Clouthier, Dennis J., "Applied Quantum Chemistry: Spectroscopic Detection and Characterization of the F₂BS and Cl₂BS Free Radicals in the Gas Phase" (2015). *Chemistry Faculty Publications*. 41.

https://uknowledge.uky.edu/chemistry_facpub/41

This Article is brought to you for free and open access by the Chemistry at UKnowledge. It has been accepted for inclusion in Chemistry Faculty Publications by an authorized administrator of UKnowledge. For more information, please contact UKnowledge@lsv.uky.edu.

Applied Quantum Chemistry: Spectroscopic Detection and Characterization of the F₂BS and Cl₂BS Free Radicals in the Gas Phase

Notes/Citation Information

Published in *The Journal of Chemical Physics*, v. 142, no. 12, article 124301, p. 124301-1 through 124301-11.

Copyright 2015 American Institute of Physics. This article may be downloaded for personal use only. Any other use requires prior permission of the author and the American Institute of Physics.

The following article appeared in *The Journal of Chemical Physics*, v. 142, no. 12, article 124301, p. 1-11 and may be found at <http://dx.doi.org/10.1063/1.4915126>

Digital Object Identifier (DOI)

<http://dx.doi.org/10.1063/1.4915126>

Applied quantum chemistry: Spectroscopic detection and characterization of the F₂BS and Cl₂BS free radicals in the gas phase

Bing Jin,¹ Phillip M. Sheridan,² and Dennis J. Clouthier^{1,a)}

¹Department of Chemistry, University of Kentucky, Lexington, Kentucky 40506-0055, USA

²Department of Chemistry and Biochemistry, Canisius College, Buffalo, New York 14208, USA

(Received 29 January 2015; accepted 5 March 2015; published online 23 March 2015)

In this and previous work [D. J. Clouthier, *J. Chem. Phys.* **141**, 244309 (2014)], the spectroscopic signatures of the X₂BY (X = H, halogen, Y = O, S) free radicals have been predicted using high level *ab initio* theory. The theoretical results have been used to calculate the electronic absorption and single vibronic level (SVL) emission spectra of the radicals under typical jet-cooled conditions. Using these diagnostic predictions, the previously unknown F₂BS and Cl₂BS free radicals have been identified and characterized. The radicals were prepared in a free jet expansion by subjecting precursor mixtures of BF₃ or BCl₃ and CS₂ vapor to an electric discharge at the exit of a pulsed molecular beam valve. The $\tilde{B}^2A_1-\tilde{X}^2B_2$ laser-induced fluorescence spectra were found within 150 cm⁻¹ of their theoretically predicted positions with vibronic structure consistent with our Franck-Condon simulations. The \tilde{B}^2A_1 state emits down to the ground state and to the low-lying \tilde{A}^2B_1 excited state and the correspondence between the observed and theoretically derived SVL emission Franck-Condon profiles was used to positively identify the radicals and make assignments. Excited state Coriolis coupling effects complicate the emission spectra of both radicals. In addition, a forbidden component of the electronically allowed $\tilde{B}-\tilde{X}$ band system of Cl₂BS is evident, as signaled by the activity in the *b*₂ modes in the spectrum. Symmetry arguments indicate that this component gains intensity due to a vibronic interaction of the \tilde{B}^2A_1 state with a nearby electronic state of ²B₂ symmetry. © 2015 AIP Publishing LLC. [<http://dx.doi.org/10.1063/1.4915126>]

I. INTRODUCTION

Free radicals of the general formula X₂BY (X = H, D or halogen, Y = O, S) are little known, although boron-containing free radicals are important intermediates in a variety of contexts. For example, boron has been characterized as a key element in radical reactions where organoboron species are used as radical initiators, chain-transfer reagents, and radical precursors.¹ In addition, boron halides and simple boranes are used as boron sources in chemical vapor deposition processes for the production of boron nitrides, carbides, and amorphous boron thin films and boron-centered free radicals are likely intermediates in such processes. The high temperature chemistry of boron rocket fuel additives also involves free radical reactions.² Discoveries of new boron-containing free radicals are both relevant and significant in all these areas of chemistry. In the present work, aided by *ab initio* predictions of their spectroscopic properties, we report the first detection of two new species, the planar F₂BS and Cl₂BS free radicals.

The only X₂BY radicals previously known were the F₂BO and H₂BO species. In 1965, Mathews and Innes³ presented spectroscopic evidence that F₂BO was the mostly likely source of an emission band system at 580 nm that was obtained from discharges through BF₃/O₂ mixtures. In 1966, Mathews⁴ showed that a group of closely spaced red-degraded emission

bands at 446.5 nm obtained in the same discharge was also due to F₂BO (or possibly F₂BO⁺). The author could not definitively establish if the 580 nm and 446.5 nm bands had a common electronic state or if either band system involved transitions to the ground state. Subsequently, Dixon *et al.*⁵ compared these bands with those of F₂CN and eliminated F₂BO⁺ as a possible source of the 580 and 446.5 nm band systems. Finally, in 1988, Jacox⁶ reconsidered Mathews' data and postulated that the 446.5 nm system was due to the ¹2A₁ → \tilde{X}^2B_2 transition and that the 580 nm bands were transitions from the same upper state to a low-lying excited state (¹2A₁ → ¹2B₁), assignments which were subsequently supported by detailed *ab initio* calculations.⁷

In 2014, we reported the first laser-induced fluorescence (LIF) and emission spectra of jet-cooled F₂¹¹BO and F₂¹⁰BO obtained by laser excitation of the bands near 446.5 nm.⁸ F₂BO was generated in a pulsed discharge jet apparatus, using a precursor mixture of 7% BF₃ and 7% O₂ in high pressure argon. The emission spectrum obtained by laser excitation of the 0-0 band clearly showed transitions down to the ground state and a second set of bands down to the low-lying excited state, precisely as postulated by Jacox.⁶ Our combined experimental and *ab initio* results proved conclusively that the previously reported emission spectra^{4,5} were due to F₂BO and substantially extended our knowledge of the structure, vibrational frequencies, and electronic states of this interesting free radical.

The only other study of an X₂BY radical was the 1976 report by Graham and Weltner⁹ of the detection of the

^{a)}Author to whom correspondence should be addressed. Electronic mail: dclaser@uky.edu

H₂BO radical among the products produced by vaporizing and trapping elemental boron in solid argon at 4–10 K. It was identified by its ESR spectrum, which was very similar to that of the isoelectronic H₂CN free radical.¹⁰ No further experimental observations of H₂BO species have been reported and the Cl₂BO, Br₂BO, H₂BS, F₂BS, Cl₂BS, and Br₂BS free radicals have never been previously observed.

In anticipation of the possibility of finding new X₂BY radicals, Clouthier¹¹ conducted an extensive *ab initio* study of the ground and first two excited electronic states of the H₂BO, H₂BS, F₂BO, and F₂BS free radicals and their various isotopologues. The radicals were found to have planar C_{2v} geometries in the \tilde{X}^2B_2 ground state, the low-lying \tilde{A}^2B_1 first excited state, and the higher \tilde{B}^2A_1 state. The most promising method of identifying these species in the gas phase was suggested to be absorption or laser-induced fluorescence spectroscopy through the allowed $\tilde{B} - \tilde{X}$ transitions which occur in the visible-near UV region of the electromagnetic spectrum. Complete basis set extrapolations of CCSD(T)/aug-cc-pVXZ (X = 3,4,5) energies were used to accurately predict the excited state energies. Franck-Condon profiles of the absorption and emission spectra and the rotational structure of the $\tilde{B} - \tilde{X}^0_0$ bands were simulated from the *ab initio* results. The calculated single vibronic level (SVL) emission spectra were found to provide a unique, readily recognizable fingerprint of each particular radical, facilitating the experimental identification of new X₂BY species in the gas phase. These predictions were very successfully employed in the present work to identify F₂BS and similar calculations led us to the Cl₂BS radical.

II. EXPERIMENT

F₂BS and Cl₂BS were generated in our pulsed discharge jet apparatus, which has been described elsewhere,¹² using precursor mixtures of 4% BF₃ or BCl₃ and 4% CS₂ in high pressure argon. In brief, the precursor gas was injected with a pulsed valve into an evacuated flow channel in a vacuum chamber. At the appropriate time, the gas pulse was subjected to a pulsed electric discharge between a pair of stainless steel ring electrodes placed in the flow channel, fragmenting the precursor molecules and producing products. A short 1 cm long reheat tube¹³ was added to the flow channel downstream of the electrodes to increase the number of collisions and enhance the production of the radicals. Natural abundance BF₃ or BCl₃ (80% ¹¹B and 20% ¹⁰B, Matheson) were used to measure transitions for the boron-11 isotopologue, while isotopically enriched ¹⁰BF₃ (96%, Ceradyne Boron Products) was used for measurements on F₂¹⁰BS. ¹⁰BCl₃ was synthesized by the reaction of gaseous ¹⁰BF₃ with powdered AlCl₃ at elevated temperatures, in a modified literature procedure,¹⁴ and used for studies of Cl₂¹⁰BS.

Approximately, 1 cm downstream of the reheat tube, the free jet expansion was interrogated with the beam of a tunable dye laser (Nd:YAG pumped Lumonics HD-500) to obtain modest resolution (~0.1 cm⁻¹) LIF spectra. The fluorescence was imaged onto the photocathode of a high-gain photomultiplier (EMI 9816QB), and the pulsed signals were processed with a gated integrator, digitized by a National

Instruments A/D board, and recorded with LabVIEW based software. The LIF spectra were calibrated to ±0.1 cm⁻¹ using a portion of the laser beam to simultaneously record the neon and argon optogalvanic spectra using hollow cathode lamps.

For low-resolution SVL emission spectra, fluorescence was generated by pumping the maximum of an LIF band and then the emission was focused through *f*/1.5 optics onto the entrance slit of a scanning monochromator (Spex 500M). The spectra were calibrated to an estimated ±1 cm⁻¹ accuracy using emission lines from an argon-filled hollow cathode lamp. The monochromator was equipped with an 1800 lines/mm grating blazed at 400 nm and operated with a bandpass of 0.2–0.8 nm.

The BS₂ radical was also produced in our discharge and its strong fluorescence interfered with our studies of the LIF spectra. As in previous work,⁸ we used both time-gating and synchronously scanning (sync-scan) LIF techniques to isolate the signals of the radicals of interest. The sync-scan LIF method used a monochromator as a tunable bandpass filter by synchronously scanning the monochromator and the excitation laser with a fixed wavenumber offset between the two. In this fashion, we were able to isolate fluorescence from the species of interest, largely free of impurity emission.

III. RESULTS AND ANALYSIS

A. *Ab initio* calculations on Cl₂BS

Our success in identifying F₂BS based on *ab initio* predictions of the LIF and emission spectra¹¹ (*vide infra*) encouraged us to undertake similar theoretical studies of Cl₂BS. Due to the larger number of electrons, these were not as extensive as the complete basis set extrapolations previously performed for the smaller H₂BO, H₂BS, F₂BO, and F₂BS radicals,¹¹ but were of sufficient quality to lead to unambiguous predictions of the expected spectra. In the present work, the ground and two lowest energy excited electronic states were examined with density functional theory (DFT) using the Becke 3-parameter exchange and Lee-Yang-Parr correlation (B3LYP) hybrid functional^{15,16} and coupled cluster theory with singles, doubles, and perturbatively included triples [CCSD(T)] using Dunning's correlation consistent basis sets augmented with diffuse functions¹⁷ (aug-cc-pVnZ). The basis sets for chlorine and sulfur included a further tight *d* function [aug-cc-pV(X+d)Z] which facilitated convergence.¹⁸ All the *ab initio* calculations were done with the Gaussian 09 software package.¹⁹ The three electronic states were calculated variationally by constraining the geometry to C_{2v} symmetry, with each state exhibiting a minimum on the potential energy surface. The highest level CCSD(T)/aug-cc-pV(T+d)Z vibrational frequencies and *T*₀ values are presented in Table I, with the geometric parameters relegated to Table VII. As in previous work,¹¹ the vibrational frequencies are numbered conventionally such that the vibrations are segregated by symmetry species and numbered in order of decreasing frequency within each symmetry species, so that ν_1 , ν_2 , and ν_3 are the *a*₁ modes, ν_4 is the single *b*₁ mode, and ν_5 and ν_6 are the *b*₂ modes.

The *ab initio* calculations show that the ground state electronic configuration of Cl₂BS is ... (13a₁)² (4b₁)² (9b₂)¹, which gives rise to a ²B₂ term. The 9b₂ HOMO is essentially

TABLE I. Summary of the observed vibrational fundamentals and T_0 values and the corresponding *ab initio* (in parentheses) harmonic frequencies for the various electronic states of F_2BS and Cl_2BS (in cm^{-1}).

	T_0	$\nu_1(a_1)$	$\nu_2(a_1)$	$\nu_3(a_1)$	$\nu_4(b_1)$	$\nu_5(b_2)$	$\nu_6(b_2)$	
\tilde{X}^2B_2	$F_2^{11}BS$...	1232 (1242) ^a	683 (683)	412 (410)	578 (578)	... (1398)	276 (277)
	$F_2^{10}BS$...	1275 (1285)	684 (687)	413 (410)	598 (602)	1452 (1447)	279 (279)
	$Cl_2^{11}BS$...	960 (966) ^b	462 (464)	237 (239)	... (432)	910 (922)	179 (181)
	$Cl_2^{10}BS$...	1000 (1006)	464 (464)	240 (239)	... (451)	946 (959)	180 (182)
\tilde{A}^2B_1	$F_2^{11}BS$	3 517 (3 464)	1224 (1236)	657 (660)	415 (420)	545 (545)	... (1412)	... (316)
	$F_2^{10}BS$	3 520 (3 463)	1248 (1277)	659 (666)	415 (420)	562 (568)	... (1462)	... (318)
	$Cl_2^{11}BS$	4 862 (4 769)	901 (909)	443 (453)	256 (255)	... (409)	932 (942)	231 (232)
	$Cl_2^{10}BS$	4 865 (4 768)	940 (947)	448 (453)	253 (256)	... (427)	968 (981)	231 (233)
\tilde{B}^2A_1	$F_2^{11}BS$	23 180 (23 175)	1101 (1136)	610 (617)	395 (394)	573 (579)	... (1509)	318 (319)
	$F_2^{10}BS$	23 180 (23 174)	1135 (1167)	621 (625)	399 (394)	599 (603)	... (1564)	324 (320)
	$Cl_2^{11}BS$	21 123 (21 271)	746 (756)	454 (453)	243 (240)	... (433)	960 (986)	256 (256)
	$Cl_2^{10}BS$	21 123 (21 269)	774 (787)	456 (454)	246 (242)	... (452)	998 (1027)	257 (256)

^a F_2BS CCSD(T)/aug-cc-pV5Z results from Ref. 11.^b Cl_2BS CCSD(T)/aug-cc-pVTZ results, present work.

an in-plane p orbital on the sulfur atom and can be labeled as nonbonding (n_O). The $4b_1$ second highest occupied molecular orbital (SHOMO) is the out-of-plane p orbital on the sulfur atom with some stabilization from the out-of-plane p orbital on the boron atom, and so can be termed a π_{BS} orbital. Finally, the $13a_1$ third highest occupied molecular orbital (THOMO) is a slightly bonding orbital between the boron and sulfur atoms, which can be labeled σ_{BO} . Parenthetically, we note that the ground state dipole moment of Cl_2BS is predicted to be about 0.4 D, which may make microwave observations difficult. The ν_1 and ν_5 fundamentals have appreciable infrared absorption intensities (175–270 km/mol), so it might be possible to detect Cl_2BS in matrix isolation experiments in the 800–1000 cm^{-1} region.

Promoting a single electron from the SHOMO to the HOMO produces the low-lying \tilde{A}^2B_1 state, which has a somewhat longer B–S bond length (increase of ~ 0.06 Å) due to the removal of an electron from an orbital with π bonding character between these two atoms. The \tilde{B}^2A_1 state is formed from the promotion of an electron in the THOMO to the HOMO, which can be considered an n – σ transition, which again increases the B–S bond length by 0.03–0.06 Å depending on the level of theory.

We have also used our CCSD(T)/aug-cc-pVTZ *ab initio* results to perform Franck-Condon simulations of the absorption and single vibronic level emission spectra of Cl_2BS , as an aid to the experimental identification. The simulation program, originally developed by Yang *et al.*,²⁰ and locally modified for the calculation of SVL emission spectra, requires input of the molecular structures, vibrational frequencies, and mass-weighted Cartesian displacement coordinates from the *ab initio* force fields of the two combining electronic states. Franck-Condon factors are then calculated in the harmonic approximation using the exact recursion relationships of Doktorov *et al.*²¹ taking into account both normal coordinate displacement and Duschinsky rotation effects.

B. Spectra of F_2BS

The LIF spectrum of $F_2^{11}BS$ is shown in Fig. 1. It commences with a strong 0-0 band centered at 23 178.5 cm^{-1} , fortuitously close to $T_0 = 23 175$ cm^{-1} predicted in our previous *ab initio* study.¹¹ The inset in Fig. 1 shows that the calculated 0-0 band contour, obtained from the *ab initio* rotational constants, matches experiment very well and validates our prediction that the band should follow b -type

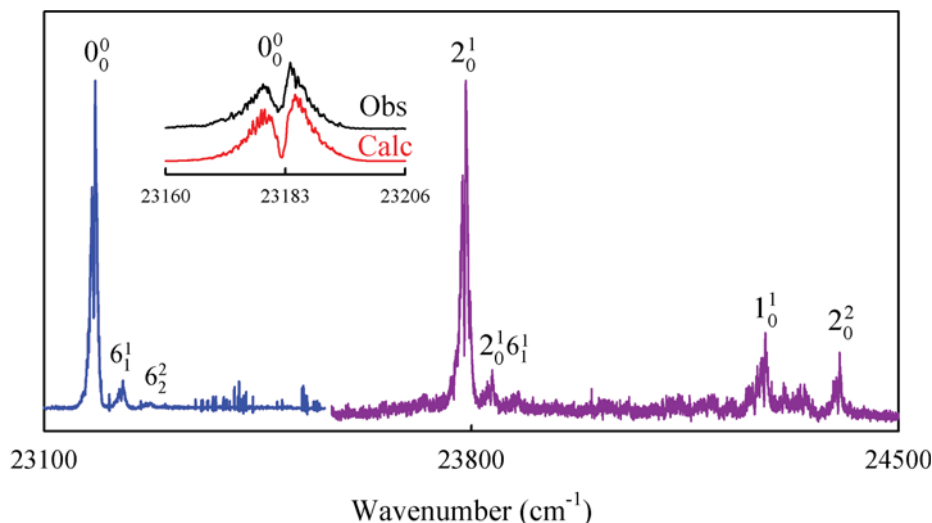


FIG. 1. The low resolution LIF spectrum of the $\tilde{B}-\tilde{X}$ transition of F_2BS . The spectrum was recorded in two sections with different laser dyes so the relative intensities of the two segments are not meaningful. The inset shows the observed and calculated (from our B3LYP/aug-cc-pV5Z results) rotational contours of the $F_2^{11}BS$ 0-0 band.

selection rules.¹¹ Our Franck-Condon simulation¹¹ of the LIF cold band spectrum shows a very strong 0-0 band, and weaker 2_0^1 and 1_0^1 bands along with a few very weak transitions and this is essentially what is observed. In addition, the experimental spectrum exhibits a few weak hot bands (2_1^1 , 3_1^1 , 6_1^1 , 6_2^2 , $2_0^1 3_1^1$, and $2_0^1 6_1^1$, not all identified in Fig. 1), analogous to those found in the spectrum of F_2BO .⁸ The LIF spectrum of $F_2^{10}BS$ is very similar to that shown in Fig. 1, although the 1_0^1 band is shifted 30 cm^{-1} to higher energy, in complete agreement with the *ab initio* isotope shift of 30 cm^{-1} . There can be little doubt that the observed LIF spectrum is the $\tilde{B}^2A_1-\tilde{X}^2B_2$ band system of F_2BS . A list of the observed LIF bands is given in Table II.

Unequivocal proof that F_2BS is the carrier of the LIF spectrum in Fig. 1 comes from the comparison of the observed and calculated 0-0 band emission spectra, shown in Fig. 2. In fact, the correspondence between the experimental spectrum and the Franck-Condon simulation is so good that the majority

of the bands were assigned directly from their simulation counterparts. The $\tilde{B}-\tilde{X}$ emission spectrum of $F_2^{11}BS$ consists of a relatively small number of bands (11) with a prominent progression in ν_1'' out to 1_2^0 , consistent with the 0.06 \AA difference in the BS bond length in the two states. The arrows in Fig. 2 highlight three features not reproduced in the simulation. Bands #2 and #3 are the 1_1^0 and 1_2^0 transitions of $F_2^{10}BS$ present in 20% natural abundance, which are resolved from the $F_2^{11}BS$ bands due to the relatively large ν_1'' (B-S stretching) isotope effect (see Table I). Both show up prominently in the spectrum of isotopically enriched $F_2^{10}BS$. Band #1 cannot be attributed to $F_2^{10}BS$, although a similar very weak band occurs 50 cm^{-1} higher in energy in the spectrum of $F_2^{10}BS$. The only other ground state vibration with frequency lower than ν_1 and with a significant boron isotope effect is ν_4 with a calculated ^{11}B frequency of 578 cm^{-1} and isotope shift of 24 cm^{-1} (see Table I). We therefore tentatively assign this transition to the 4_2^0 band, with half the interval giving

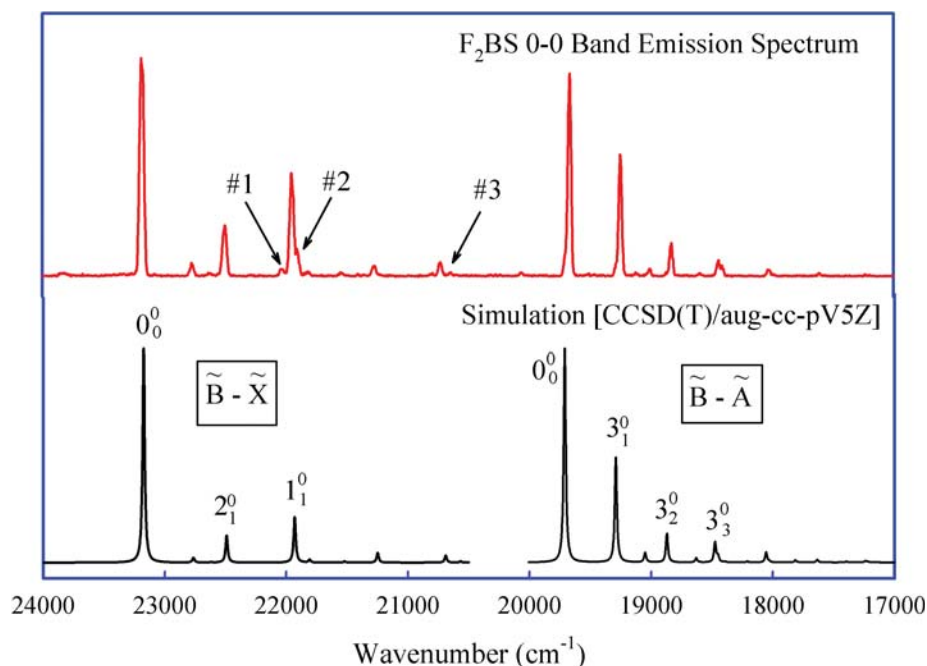


FIG. 2. The observed 0-0 band emission spectrum of F_2BS (top panel) and the corresponding harmonic Franck-Condon simulation (bottom panel). The simulations involved calculating the $\tilde{B}-\tilde{X}$ and $\tilde{B}-\tilde{A}$ spectra, separately, so there is a break in the spectrum near $20\ 300\text{ cm}^{-1}$. The relative intensities of the two calculated spectra have been normalized to the strongest feature in the corresponding emission spectrum.

TABLE II. Observed vibronic bands in the LIF spectra of the $\tilde{B}^2A_1-\tilde{X}^2B_2$ transition of the boron isotopologues of F_2BS .

Assignment	$F_2^{11}BS$		$F_2^{10}BS$	
	Transition (cm^{-1})	Interval (cm^{-1})	Transition (cm^{-1})	Interval (cm^{-1})
2_1^1	23 116.3	$0_0^0-58.5$
3_1^1	23 161.3	$0_0^0-17.2$	23 160.8	$0_0^0-14.0$
0_0^0	23 178.5	...	23 174.8	...
6_1^1	23 220.9	$0_0^0+42.4$	23 220.1	$0_0^0+45.3$
6_2^2	23 266.1	$6_1^1+45.2$
$2_0^2 3_1^1$	23 771.0	$3_1^1+609.7$	23 777.7	$3_1^1+616.9$
$2_0^2/4_0^1$	23 788.6	$0_0^0+610.1$	23 795.8	$0_0^0+621.0$
$2_0^2 6_1^1$	23 831.7	$6_1^1+610.8$	23 838.1	$6_1^1+618.0$
1_0^1	24 279.7	$0_0^0+1101.2$	24 309.9	$0_0^0+1135.1$
2_0^2	24 400.9	$2_0^1+612.3$	24 417.0	$2_0^1+621.2$

TABLE III. Emission bands (in cm^{-1}) observed by pumping the 0_0^0 and 2_0^1 absorption bands of the $\tilde{B}-\tilde{X}$ transition of F_2BS . Unassigned lines: $F_2^{10}BS$: 0-0 band spectrum 20 063(vw); 2(1,0) band spectrum 20 028 (w).

0_0^0 band emission spectrum					2_0^1 band emission spectrum				
$F_2^{11}BS$			$F_2^{10}BS$		$F_2^{11}BS$			$F_2^{10}BS$	
Assign	Transition	Interval	Transition	Interval	Assign	Transition	Interval	Transition	Interval
$\tilde{B}-\tilde{X}$ transitions ^a									
0_0^0	23 181	...	23 180	...	2_0^1	23 796	$\nu_2' = 615$	23 802	$\nu_2' = 622$
3_1^0	22 769	$\nu_3 = 412$	22 767	$\nu_3 = 413$	4_1^1	23 181	...	23 183	...
6_2^0	22 629	$2\nu_6 = 552$	22 621	$2\nu_6 = 559$	2_1^1	23 113	$\nu_2 = 683$	23 117	$\nu_2 = 685$
2_1^0	22 500	$\nu_2 = 681$	22 496	$\nu_2 = 684$	$2_1^1 3_1^0$	22 711	$\nu_3 = 402$	22 710	$\nu_3 = 407$
$4_0^2?$	22 031	$2\nu_4 = 1150$	21 981	$2\nu_4 = 1199$	$2_0^1 4_1^1$	22 506	$\nu_2 = 675$	22 501	$\nu_2 = 682$
1_1^0	21 949	$\nu_1 = 1232$	21 904	$\nu_1 = 1276$	2_2^1	22 438	$2_1^1 - 675$	22 436	$2_1^1 - 681$
2_2^0	21 811	$2_1^0 - 689$	$1_1^0 4_1^1$	21 956	$4_1^1 - 1225$	21 904	$4_1^1 - 1279$
$1_1^0 3_1^0$	21 546	$1_1^0 - 403$	21 504	$1_1^0 - 400$	$1_0^2 2_1^1$	21 884	$2_1^1 - 1229$	21 846	$2_1^1 - 1271$
$1_1^0 2_1^0$	21 273	$1_1^0 - 676$	21 227	$1_1^0 - 677$	2_3^1	21 752	$2_2^1 - 686$
$1_1^0 4_0^2?$	20 711	$1_1^0 - 1193$	$1_0^2 2_2^1$	21 214	$2_2^1 - 1224$	21 168	$2_2^1 - 1268$
1_2^0	20 728	$1_1^0 - 1221$	20 642	$1_1^0 - 1262$	$1_2^0 4_1^1$	20 641	$4_1^1 - 2542$
$5_2^0?$	20 275	$2\nu_5 = 2905$	$1_2^0 2_1^1$	20 657	$2_1^1 - 2456$	20 584	$2_1^1 - 2533$
$1_2^0 2_1^0$	20 061	$1_2^0 - 667$...	2 ...	$1_0^2 2_1^0 4_1^1$	20 028
$\tilde{B}-\tilde{A}$ transitions ^b									
0_0^0	19 664	$\tilde{X}0_0 + 3517$	19 660	$\tilde{X}0_0 + 3520$	2_0^1	20 278	$\nu_2' = 614$	20 283	$\nu_2' = 623$
3_1^0	19 249	$\nu_3 = 415$	19 245	$\nu_3 = 415$	$2_0^1 3_1^0$	19 862	$\nu_3 = 416$	19 865	$\nu_3 = 418$
2_1^0	19 004	$\nu_2 = 660$	19 006	$\nu_2 = 654$	4_1^1	19 695	...	19 699	...
3_2^0	18 829	$3_1^0 - 420$	18 828	$3_1^0 - 417$	2_1^1	19 620	$\nu_2 = 658$	19 624	$\nu_2 = 659$
$2_0^1 3_1^0$	18 592	$2_1^0 - 412$	$3_0^0 4_1^1$	19 281	$4_1^1 - 418$
1_1^0	18 440	$\nu_1 = 1224$	18 412	$\nu_1 = 1248$	$2_1^1 3_1^0$	19 206	$2_1^1 - 414$	19 207	$2_1^1 - 417$
3_3^0	18 410	$3_2^0 - 419$	$2_0^1 4_1^1$	19 037	$4_1^1 - 662$
...	2_2^1	18 962	$2_1^1 - 658$	18 966	$2_1^1 - 658$
...	$3_2^0 4_1^1$	18 863	$4_1^1 - 836$
$1_1^0 3_1^0$	18 028	$1_1^0 - 412$	17 990	$1_1^0 - 422$	$2_1^1 3_2^0$	18 792	$2_1^1 - 828$	18 791	$2_1^1 - 833$
...	$1_1^0 4_1^1$	18 442	$4_1^1 - 1257$
...	$1_1^0 2_1^1$	18 398	$2_1^1 - 1222$	18 371	$2_1^1 - 1253$
$1_1^0 3_2^0$	17 612	$1_1^0 3_1^0 - 416$	$1_1^0 2_1^1 3_1^0$	17 987

^aVibrational intervals are for the \tilde{X} state unless otherwise noted.^bVibrational intervals are for the \tilde{A} state unless otherwise noted.

$\nu_4'' = 575 \text{ cm}^{-1}$ and a 25 cm^{-1} isotope shift. The 0-0 band emission spectrum of F_2^{10}BS has many of the same features but has additional very weak bands tentatively assigned as $1_1^0 4_2^0$ and 5_2^0 . Since transitions involving two quanta of non-totally symmetric modes are expected to be very weak, all such assignments are only tentative as they could also be due to impurities or emission from higher levels excited through sequence bands overlapping the 0-0 band. A complete list of the $\tilde{B}-\tilde{X}$ emission band assignments is given in Table III.

The 0-0 band $\tilde{B}-\tilde{A}$ emission band systems of F_2^{11}BS and F_2^{10}BS were very easy to assign as they matched the simulations almost perfectly, with no extraneous features. The major progression involves ν_3 (out to 3_3^0) with a small amount of activity in ν_1 . Animations show that in the \tilde{A} state both of these modes involve substantial contributions from the BS stretching and FBF symmetric bending internal coordinates. The assignments are summarized in Table III.

We also recorded the SVL emission spectra of the 2_0^1 bands, which harbored a surprise. In this case, the emission spectra were much more complicated than the initial simulation, with some bands consisting of closely spaced doublets (particularly for F_2^{10}BS) along with a few extraneous features. Examining the \tilde{B} state calculated vibrational frequencies (Table I), it is apparent that ν_2 and ν_4 are almost degenerate, differing by 38 cm^{-1} in F_2^{11}BS and only 22 cm^{-1} in F_2^{10}BS and that Coriolis coupling between the \tilde{B} state 2^1 and 4^1 levels is the likely reason for the complexity. The 2_0^1 band emission spectrum of F_2^{10}BS is shown in Fig. 3, along with a simulation constructed by adding together Franck-Condon simulations from the 2^1 and 4^1 levels and normalizing the intensities to those of the observed 4_1^1 and 2_1^1 bands in each case. The agreement is excellent, confirming that the upper state pumped by the laser has $2^1/4^1$ character. The bands in the spectra of both isotopologues were assigned based on observed and calculated vibrational intervals and on the

relative intensities predicted by the composite simulations. These results are summarized in Table III.

C. Spectra of Cl_2BS

Our best CCSD(T)/aug-cc-pVTZ calculations predicted the $\tilde{B}-\tilde{X}$ T_0 of $\text{Cl}_2^{11}\text{BS}$ to be $21\,271 \text{ cm}^{-1}$. Substituting BCl_3 for BF_3 and using similar experimental conditions, we readily found a strong 0-0 band at $21\,123 \text{ cm}^{-1}$, 148 cm^{-1} lower than predicted. The Franck-Condon simulation of the Cl_2BS cold band absorption spectrum indicates that there should be more bands than observed in the LIF spectra of F_2BO and F_2BS , which is what is found, as shown in Fig 4. In addition to the very strong 0-0 band, there are weaker 3_0^1 , 2_0^1 , 1_0^1 , and combination bands. Furthermore, the spectra of both isotopologues exhibit weak hot bands below $21\,000 \text{ cm}^{-1}$ which can only be assigned as 3_1^0 and 6_1^0 . The latter is unprecedented in the LIF spectra of the fluorinated radicals and must be vibronically induced through mixing with another excited state. The corresponding 6_0^1 cold band is calculated to lie within the rotational envelope of the noticeably broad 3_1^0 band (FWHM: $0_0^0 \approx 9 \text{ cm}^{-1}$, $3_1^0 \approx 19 \text{ cm}^{-1}$). In addition, $\text{Cl}_2^{11}\text{BS}/\text{Cl}_2^{10}\text{BS}$ shows a weak band $960/998 \text{ cm}^{-1}$ above the 0_0^0 band which is assigned as the vibronically induced 5_0^1 band, based on detailed consideration of the emission data (*vide infra*). Of course, ν_5' has the same vibrational symmetry as ν_6' , so it is perhaps not too surprising that 5_0^1 also appears in the Cl_2BS spectrum. Finally, the Cl_2BS least moment of inertia (I_a) is in the molecular plane perpendicular to the B-S bond, so the bands should follow *a*-type selection rules and not exhibit the central minima found for F_2BS (see Fig. 1), and this is what is observed. The assignments of the LIF spectra are given in Table IV along with some derived vibrational intervals.

The substantial number of bands in the LIF spectra provided the opportunity to obtain many more SVL emission

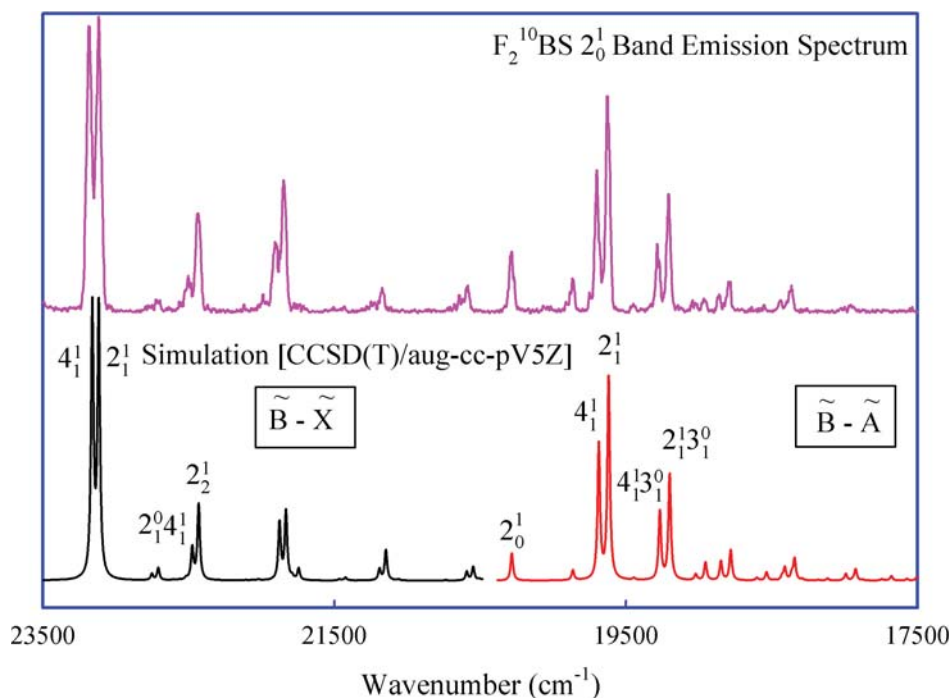


FIG. 3. The F_2^{10}BS 2_0^1 band emission spectrum (top panel) and the corresponding harmonic Franck-Condon simulation (bottom panel). The simulation was obtained by adding together Franck-Condon simulations of emission spectra from the 2^1 and 4^1 levels and normalizing the intensities to those of the observed 4_1^1 and 2_1^1 bands in each case.

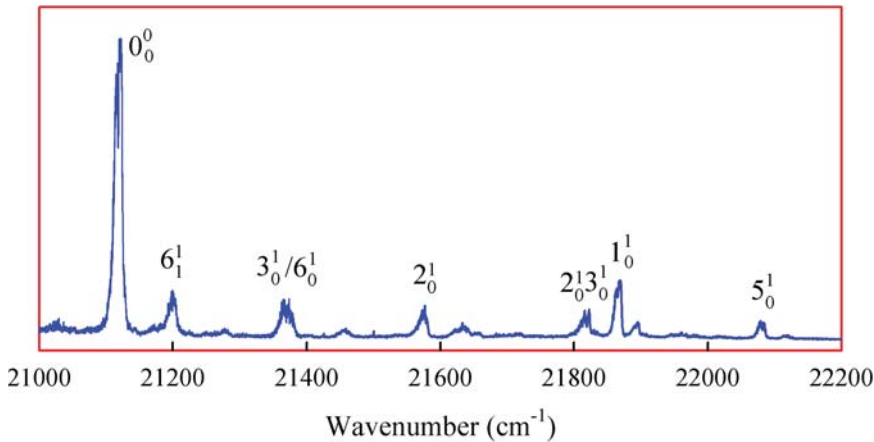


FIG. 4. A portion of the low resolution LIF spectrum of the $\tilde{B}-\tilde{X}$ transition of Cl_2BS . The 3(1,0) and 6(1,0) bands are overlapped, giving rise to a feature that appears to be broader than any other in the spectrum.

spectra than in the F_2BO and F_2BS cases. For each isotopologue, we recorded dispersed emission spectra by pumping the 3_1^0 , 6_1^0 , 0_0^0 , 6_1^1 , $3_0^1/6_0^1$, $6_1^1 3_0^1$, 2_0^1 , 1_0^1 , and 5_0^1 LIF bands, along with the $2_0^1 3_0^1$ band of $\text{Cl}_2^{11}\text{BS}$ and the 6_0^2 band of $\text{Cl}_2^{10}\text{BS}$. We will not discuss the details of all these spectra but simply refer to a few cases which illustrate the salient points of the analysis.

The 0-0 band emission spectrum of $\text{Cl}_2^{11}\text{BS}$ is shown in Fig. 5 along with our Franck-Condon simulation. It is readily apparent that the simulation is substantially at odds with experiment for the $\tilde{B}-\tilde{X}$ band system but is in quite good agreement for the $\tilde{B}-\tilde{A}$ transitions. The small features labeled #1, #2 and #3 are the key to understanding this behavior. Transitions #1 and #2 are to higher energy than the 0-0 band that was pumped by the laser and are readily assigned as 3_1^0 and 6_1^1 , both bands that are also observed in the LIF spectra. We conclude that the 0-0 band is overlapped by the 3_1^0 sequence band (it is calculated from the known vibrational frequencies to occur within the rotational contour of the 0-0 band) and that the 3^1 ($\nu_3 = 244 \text{ cm}^{-1}$) and 6^1 ($\nu_6 = 259 \text{ cm}^{-1}$) levels are Coriolis coupled. A similar complication was found in the

spectrum of F_2BO .⁸ This conclusion is buttressed by the fact that pumping the Cl_2BS 6_1^1 band yields an emission spectrum that includes a weak 3_1^0 band. Thus, the 0-0 band emission spectrum in Fig. 5 contains contributions from the \tilde{B} state 0_0^0 , 3^1 , and 6^1 levels, accounting for the deviations from the harmonic Franck-Condon simulation. In addition to the bands predicted by the Franck-Condon simulation, we have also assigned a weak vibronically induced 6_1^0 band and an even weaker $1_1^0 6_1^0$ band.

Initially, further $\text{Cl}_2^{11}\text{BS}/\text{Cl}_2^{10}\text{BS}$ zero-point $\tilde{B}-\tilde{X}$ emission bands of medium intensity with ground state intervals of $907/949 \text{ cm}^{-1}$ were difficult to assign. However, once it was recognized that the strongest features of the emission spectra of the LIF bands at $22\,078.3/22\,114.3 \text{ cm}^{-1}$ (Table IV) had the same intervals, it became apparent that these were the ν_3'' frequencies, with a boron isotope shift of 42 cm^{-1} , comparable to the *ab initio* value of 37 cm^{-1} . This assignment was confirmed by the presence of weak transitions down to the $1_1 5_1$ level in the 0_0^0 and 1_0^1 band emission spectra with observed $\nu_1 + \nu_5$ frequency isotope shifts of 79 cm^{-1} in both spectra. The expected isotope shift (from combining the observed shifts of

TABLE IV. Observed vibronic bands in the LIF spectra of the $\tilde{B}^2A_1-\tilde{X}^2B_2$ transition of the boron isotopologues of Cl_2BS .

Assignment	$\text{Cl}_2^{11}\text{BS}$		$\text{Cl}_2^{10}\text{BS}$	
	Transition (cm^{-1})	Interval (cm^{-1})	Transition (cm^{-1})	Interval (cm^{-1})
3_1^0	20 881.3	$\nu_3'' = 237.3$	20 878.8	$\nu_3'' = 237.5$
6_1^0	20 943.9	$\nu_6'' = 174.7$	20 940.0	$\nu_6'' = 176.3$
0_0^0	21 118.6	...	21 116.3	...
6_1^1	21 199.4	$\nu_6 = 255.5$	21 195.2	$\nu_6 = 255.2$
6_2^2	21 278.1	$6_1^1 + 82.9$
3_0^1 and 6_0^1	21 370.5	...	21 368.9	...
$3_0^1 6_1^1$	21 453.5	$6_1^1 + 254.1$	21 452.9	$6_1^1 + 257.7$
2_0^1	21 572.2	$\nu_2 = 453.6$	21 572.3	$\nu_2 = 456.0$
6_0^2 and $3_0^2?$	21 633.9	...	21 632.6	...
$2_0^1 3_0^1$	21 817.2	$2_0^1 + 245.0$	21 814.1	$2_0^1 + 241.8$
1_0^1	21 863.9	$\nu_1 = 745.3$	21 889.8	$\nu_1 = 773.5$
5_0^1	22 078.3	$\nu_5 = 959.7$	22 114.3	$\nu_5 = 998.0$
$2_0^1 3_0^1?$	22 266.3	$2_0^1 3_0^1 + 449.1$
$1_0^1 2_0^1$	22 311.6	$2_0^1 + 739.4$

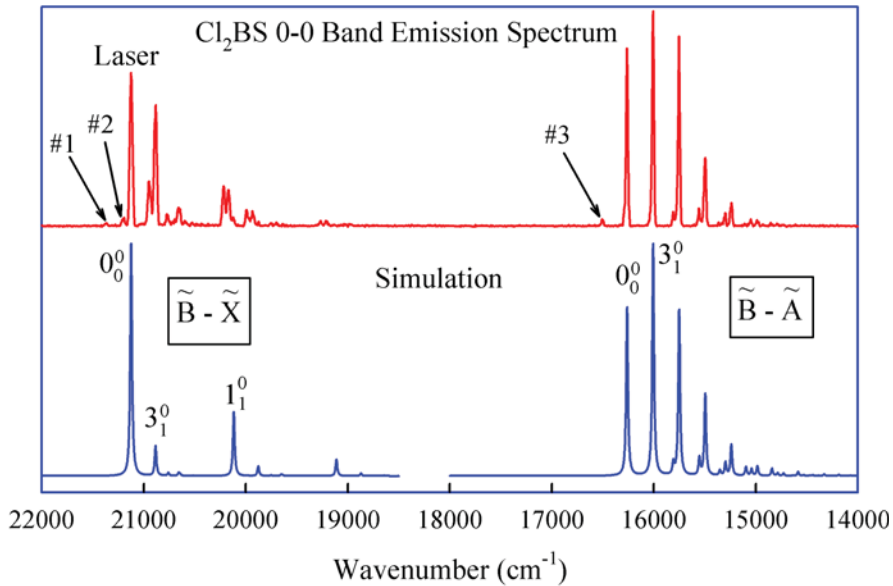


FIG. 5. The observed 0-0 band emission spectrum of Cl_2BS (top panel) and the corresponding harmonic Franck-Condon simulation (bottom panel). The simulations involved calculating the $\tilde{B}-\tilde{X}$ and $\tilde{B}-\tilde{A}$ spectra, separately, so there is a break in the spectrum near $18\,500\text{ cm}^{-1}$. The relative intensities of the two calculated spectra are not meaningful.

TABLE V. Emission bands observed by pumping the 0_0^0 band of the $\tilde{B}-\tilde{X}$ transition of Cl_2BS .

Assignment	$\text{Cl}_2^{11}\text{BS}$		$\text{Cl}_2^{10}\text{BS}$	
	Transition (cm^{-1})	Interval (cm^{-1})	Transition (cm^{-1})	Interval (cm^{-1})
$\tilde{B}-\tilde{X}^a$				
3_0^1	21 367	$\nu_3' = 244$	21 374	$\nu_3' = 251$
6_1^1	21 203	$\nu_6' = 259$	21 200	$\nu_6' = 259$
0_0^0	21 123	...	21 123	...
6_1^0	20 944	$\nu_6 = 179$	20 942	$\nu_6 = 181$
3_1^0	20 886	$\nu_3 = 237$	20 883	$\nu_3 = 240$
6_2^0	20 768	$6_1^0 - 176$	20 764	$6_1^0 - 178$
2_1^0	20 654	$\nu_2 = 469$	20 658	$\nu_2 = 465$
5_1^0	20 216	$\nu_5 = 907$	20 174	$\nu_5 = 949$
1_1^0	20 167	$\nu_1 = 956$	20 121	$\nu_1 = 1002$
$1_1^0 6_1^0$	19 992	$1_1^0 - 175$	19 945	$1_1^0 - 176$
$1_1^0 3_1^0$	19 927	$1_1^0 - 240$	19 884	$1_1^0 - 237$
$1_1^0 5_1^0$	19 263	$1_1^0 - 904$	19 184	$1_1^0 - 937$
1_2^0	19 209	$1_1^0 - 958$	19 135	$1_1^0 - 986$
$1_1^0 3_1^0 5_1^0$	18 954	$1_1^0 5_1^0 - 230$
$\tilde{B}-\tilde{A}^b$				
3_0^1	16 504	$\nu_3' = 243$	16 504	$\nu_3' = 246$
0_0^0	16 261	$\tilde{X} 0_0 + 4862$	16 258	$\tilde{X} 0_0 + 4865$
3_1^0	16 005	$\nu_3 = 256$	16 005	$\nu_3 = 253$
$2(0,1)$	15 809	$\nu_2 = 452$	15 813	$\nu_2 = 445$
3_2^0	15 753	$3_1^0 - 252$	15 750	$3_1^0 - 255$
$2_1^0 3_1^0$	15 557	$3_1^0 - 448$	15 555	$3_1^0 - 450$
3_3^0	15 495	$3_2^0 - 258$	15 494	$3_2^0 - 256$
$2_1^0 3_2^0$	15 301	$3_2^0 - 452$	15 303	$3_2^0 - 447$
3_4^0	15 239	$3_3^0 - 256$	15 238	$3_3^0 - 256$
$2_1^0 3_3^0$	15 045	$3_3^0 - 450$	15 051	$3_3^0 - 443$
3_5^0	14 986	$3_4^0 - 253$	14 986	$3_4^0 - 252$

^aVibrational intervals are for the \tilde{X} state unless otherwise noted.

^bVibrational intervals are for the \tilde{A} state unless otherwise noted.

ν_1'' and ν_5'') is 78 cm^{-1} whereas the *ab initio* value is 77 cm^{-1} , both in good agreement with experiment. The 0_0^0 band $\tilde{B}-\tilde{X}$ emission assignments are summarized in Table V.

Although the excellent agreement between Franck-Condon simulation and experiment (Fig. 5) shows that most of the intensity of the $\tilde{B}-\tilde{A}$ band system originates from the 0^0 level, the weak feature labeled #3 is not in the calculated spectrum, but was readily assigned as the 3_0^1 band. There is no evidence for any vibronically induced features in the $\tilde{B}-\tilde{A}$ spectrum. The most intense bands form a progression in ν_3'' out to 3_5^0 , along with weaker bands involving ν_2'' and $\nu_2'' + \nu_3''$ combinations. These are listed in Table V.

Other emission spectra with upper states involving either ν_3' or ν_6' have similar complications due to the Coriolis coupling of these two modes. Most of the remaining emission spectra were understandable and assignable based on the assumption of laser excitation of a single uncompromised vibrational level, such as 1^1 or 2^1 , with only modest deviations from the calculated spectra in the harmonic approximation, due to vibronically induced bands. Generally, it was found that the strongest features in the emission spectra of LIF bands involving an upper state fundamental (1_0^1 , 2_0^1 , etc.) were down to one quantum of the same fundamental in the ground state, in accord with expectations based on the Franck-Condon principle. Thus, the most intense $\tilde{B}-\tilde{X}$ emission bands from laser excitation of the 1^1 , 2^1 , 3^1 , 5^1 , and 6^1 levels were 1_1^1 , 2_1^1 , 3_1^1 , 5_1^1 , and 6_1^1 , respectively.

From the analysis of the LIF and emission spectra, we have obtained most of the fundamental frequencies in the three combining states, as reported in Table I. Some of these values deserve further comment. The \tilde{B} state ν_6 frequencies were obtained from the 6_1^1 to 6_0^1 LIF band intervals and the ground state ν_6 from the emission 0_0^0 to 6_0^1 differences. The \tilde{A} state ν_6 values were calculated from the emission spectra as $0_0^0 (\tilde{B}-\tilde{A}) + \nu_6' - 6_1^1 (\tilde{B}-\tilde{A})$ and the ν_5 values were derived in a similar fashion. The \tilde{B} state ν_3 values were taken as the differences between the $\tilde{B}-\tilde{A}$ 3_0^1 and 0_0^0 bands observed in the 0-0 band emission spectra, as the LIF values are compromised by the overlap of the 3_0^1 and 6_0^1 bands. In addition, a variety of Cl_2BS \tilde{X} and \tilde{A} state overtone and combination levels were measured and assigned and these are collected in Table VI.

IV. DISCUSSION

A. Comparison to theory

The theoretical and experimental results are compared in Table I. It is apparent that the calculated band origins for the two electronic excited states are in excellent agreement with experiment, differing by a minimum of 5 cm^{-1} (0.02%) for the \tilde{B} state of F_2BS and a maximum of 148 cm^{-1} (0.70%) for the \tilde{B} state of Cl_2BS . We have previously¹¹ attributed a similar fortuitously good level of agreement in F_2BO to the small geometry changes on electronic excitation, the lack of spin contamination, and the predominantly single reference character of the wavefunctions, factors which also apply in the present cases. The measured vibrational fundamentals are very consistent with our CCSD(T)/aug-cc-pVnZ harmonic vibrational frequencies, with a maximum deviation of 35 cm^{-1}

TABLE VI. The observed overtone and combination vibrational intervals (in cm^{-1}) for the \tilde{X} and \tilde{A} electronic states of Cl_2BS .

	\tilde{X}^2B_2		\tilde{A}^2B_1	
	$\text{Cl}_2^{11}\text{BS}$	$\text{Cl}_2^{10}\text{BS}$	$\text{Cl}_2^{11}\text{BS}$	$\text{Cl}_2^{10}\text{BS}$
$2\nu_6$	355	355
$2\nu_3$	476	487	510	509
$\nu_3 + 2\nu_6$...	596
$\nu_2 + \nu_6$	631	633
$\nu_2 + \nu_3$	700	702	704	703
$3\nu_3$	766	764
$2\nu_2$	930	933	893	904
$\nu_2 + 2\nu_3$	935	...	960	958
$4\nu_3$	1021	1020
$\nu_5 + \nu_6$	1088	1121
$\nu_3 + \nu_5$	1153	1181	1212	1249
$\nu_1 + \nu_6$	1136	1178
$2\nu_2 + \nu_3$	1150	1155
$\nu_1 + \nu_3$	1197	1244	1155	1195
$\nu_2 + 3\nu_3$	1216	1216
$5\nu_3$	1275	1272
$\nu_2 + \nu_5$	1368	1400
$\nu_1 + \nu_2$	1417	1460	1351	1390
$2\nu_2 + 2\nu_3$	1398	...
$\nu_1 + 2\nu_3$	1412	1453
$\nu_2 + 4\nu_3$	1460	...
$2\nu_3 + \nu_5$	1464	1517
$\nu_2 + \nu_3 + \nu_5$	1600	1636	1661	...
$\nu_1 + \nu_2 + \nu_3$	1654	1698	1605	1649
$\nu_1 + 3\nu_3$	1665	1708
$3\nu_3 + \nu_5$	1720	1753
$2\nu_5$	1811	1875
$\nu_1 + \nu_2 + 2\nu_3$	1857	...
$\nu_1 + \nu_5$	1859	1933
$2\nu_1$	1914	1991
$\nu_1 + 4\nu_3$	1919	1960
$4\nu_3 + \nu_5$	1969	...
$\nu_3 + 2\nu_5$	2044	2116
$2\nu_1 + \nu_6$	2084	2165
$2\nu_1 + \nu_3$	2153	2228
$3\nu_1$	2853	2971

(3%) and an average error of only 7 cm^{-1} . The observed isotope shifts are also in excellent agreement with those calculated experimentally. Most importantly, the harmonic Franck-Condon simulations, which hinge on reliable molecular geometries, vibrational frequencies, and normal mode Cartesian displacement coordinates of the two combining electronic states, mimic experiment so well that they provide unambiguous identification of the emitting species and reliable assignments for the great majority of the emission bands.

B. Molecular structures

Since the spectra of F_2BO , F_2BS , and Cl_2BS are too congested for detailed rotational analysis, we must rely on the *ab initio* results to compare molecular geometries. The fact that the calculated rotational contours of the F_2BO and F_2BS $\tilde{B}-\tilde{X}$ 0_0^0 bands match experiment very well and that the Franck-Condon simulations agree so well with experiment in cases uncomplicated by extensive Coriolis or vibronic

TABLE VII. The *ab initio* ground state molecular structures of the known gas phase X_2BY free radicals and the calculated changes in geometry on electronic excitation.

Parameter		F ₂ BO ^a	F ₂ BS ^a	Cl ₂ BS ^b
\tilde{X}^2B_2	BY (Å)	1.3639	1.8019	1.7801
	BX (Å)	1.3135	1.3168	1.7544
	XBX (°)	119.29	120.56	120.89
\tilde{A}^2B_1	Δ [BY] (Å)	+0.042	+0.048	+0.068
	Δ [BX] (Å)	+0.002	+0.004	-0.007
	Δ [XBX] (°)	+1.44	-0.69	-2.23
\tilde{B}^2A_1	Δ [BY] (Å)	+0.011	+0.058	+0.064
	Δ [BX] (Å)	-0.006	-0.018	-0.021
	Δ [XBX] (°)	-0.09	+2.57	+4.93

^aCCSD(T)/aug-cc-pV5Z values from Ref. 11.^bCCSD(T)/aug-cc-pVTZ values from this work.

coupling suggest that the *ab initio* structures are reasonably reliable. The structures obtained from theory are compared in Table VII. It is important to emphasize that each radical is predicted to be planar and of C_{2v} symmetry in all three electronic states.

It is immediately evident that the ground state bond angles in all three radicals are very similar and very close to the 120° value expected in the simplest approximation of sp^2 hybridization on the central boron atom. The BF bond lengths are almost identical in F₂BO and F₂BS, but the BS bond length of Cl₂BS is 0.02 Å shorter than that of F₂BS. The BF (1.31-1.32 Å) and BCl (1.754 Å) bond lengths are comparable to the bond lengths of BF₃ (1.307 Å) and BCl₃ (1.74 Å), respectively.^{22,23}

Our LIF spectra reflect the changes in the molecular structure between the ground state and the \tilde{B}^2A_1 electronic excited state. Table VII shows that F₂BO undergoes very little geometry change and the LIF and absorption spectra consist of a prominent 0_0^0 band and little else. In F₂BS, the BS bond length elongates by about 0.06 Å and the bond angle opens by about 2.5°, resulting in additional absorption transitions to the 2¹ and 1¹ states, vibrations which both involve substantial BS stretching motions. In Cl₂BS, the changes are more global with a 0.06 Å elongation of the BS bond, a 0.02 Å decrease in the BCl bond length and an increase in the bond angle by 5°, which leads to activity in ν_1' (BS stretch), ν_2' (BCl stretch), and ν_3' (CIBCl bend).

The observed $\tilde{B}-\tilde{A}$ emission spectra reflect the geometric changes between the \tilde{B} and \tilde{A} states. These can be determined from the data in Table VII by taking the difference between the Δ values of the two states. For example, for F₂BS, we have $\Delta BS = \Delta[BX]_{\tilde{A}} - \Delta[BX]_{\tilde{B}} = 0.048 - 0.058 = 0.01$ Å. It is then immediately apparent that the only significant change is in the F₂B or Cl₂B bond angle, which accounts for the pronounced activity in the \tilde{A} state ν_3 (symmetric bend or scissors) mode in all the spectra.

C. Vibronic coupling

Although the observed spectra of F₂BO and F₂BS show no evidence of vibronic coupling, the $\tilde{B}^2A_1-\tilde{X}^2B_2$ allowed

electronic transition of Cl₂BS clearly contains forbidden components which gain intensity by vibronic coupling through the b_2 vibrations. Vibronic coupling can only occur between states that differ by no more than the species of one of the normal vibrations.²⁴ The involvement of the b_2 vibration implies that the 2A_1 state is coupled to a nearby 2B_2 state. Although it is, in principle, possible for the vibronic coupling to occur with the \tilde{X}^2B_2 ground state, it is so energetically distant (2.6 eV) that it is unlikely to be involved. Therefore, it must be that there is an excited 2B_2 electronic state of Cl₂BS sufficiently close to the \tilde{B} state to cause the vibronic perturbations and that such a state does not substantially perturb the second excited state in the fluorinated compounds. Although no detailed calculations are available for the higher excited electronic states of Cl₂BS, MRCI calculations on the vertical spectrum of the isoelectronic H₂CO⁺ species²⁵ predict a 2B_2 ($2b_2 \leftarrow 1b_2$) state about 1 eV above the \tilde{B}^2A_1 state, ideally situated for vibronic coupling. Similarly, in F₂CO⁺, the 2B_2 state is within 0.3 eV of the 1^2A_1 state (calculated at the optimized ground state geometry of F₂CO) and within 0.8 eV according to the adiabatic ionization potentials from the photoelectron spectrum.²⁶ Of course, the $^2B_2-\tilde{X}^2B_2$ transition is also electronically allowed and so the forbidden component of the $\tilde{B}-\tilde{X}$ system of Cl₂BS can, at least in theory, gain intensity from the former by Herzberg-Teller intensity stealing. Detailed calculations of the identities and energies of the higher excited states of the X_2BY radicals will be required to further elaborate this point.

The \tilde{A}^2B_1 state cannot have a vibronic interaction with the nearby \tilde{X}^2B_2 state as C_{2v} molecules do not have a normal mode of a_2 symmetry.²⁴ In a similar fashion, although the evidence shows that the \tilde{B}^2A_1 state has an admixture of another 2B_2 state, this vibronic perturbation cannot lead to the occurrence of forbidden components in the $\tilde{B}^2A_1-\tilde{A}^2B_1$ emission band system and no such vibronically induced bands have been observed in the spectra of F₂BO, F₂BS, or Cl₂BS.

V. CONCLUSIONS

In the present case, high level *ab initio* theory has proven to be a powerful tool for predicting the spectroscopic signatures of new X_2BY free radicals, leading to their experimental detection in the gas phase. The Franck-Condon simulations of the emission spectra, in particular, were used to provide unambiguous identification of the radicals and, in most cases, reliable assignments of the observed transitions. The observed spectra of F₂BS are complicated by Coriolis coupling of the ν_2 and ν_4 modes in the excited state, so the 2_0^1 band emission spectrum exhibits transitions from both upper state levels. Even here, theory does very well—a composite Franck-Condon simulation of emission from 2¹ and 4¹ matches experiment very satisfactorily.

The LIF spectrum of Cl₂BS exhibits more vibronic activity than those of F₂BO and F₂BS, a necessary consequence of the larger geometric distortion of Cl₂BS on $\tilde{B}^2A_1-\tilde{X}^2B_2$ electronic excitation predicted by the *ab initio* calculations. In addition, Cl₂BS exhibits clear evidence of the existence of a forbidden component of the allowed electronic transition in

the experimental spectrum, involving activity in the b_2 modes, ν_5 and ν_6 . This subset of the observed bands gains intensity by Herzberg-Teller intensity stealing from a nearby allowed transition, which is most likely $2^2B_2-\tilde{X}^2B_2$. Finally, the Cl_2BS emission spectra are complicated by Coriolis coupling of ν_3 and ν_6 in the \tilde{B} state. Both the excited state Coriolis coupling and vibronic interactions lead to complications in the $\tilde{B}-\tilde{X}$ emission spectra that cannot be accounted for in the harmonic Franck-Condon simulations. However, the $\tilde{B}-\tilde{A}$ band systems are largely free of such complexity and are reproduced by the simulations with gratifying fidelity.

ACKNOWLEDGMENTS

The research of the Clouthier group was supported by the National Science Foundation. P.M.S. would like to thank the Clouthier group for hosting his sabbatical leave.

- ¹P. Renaud, A. Beauseigneur, A. Brecht-Forster, B. Becattini, V. Darmency, S. Kandhasamy, F. Montermini, C. Ollivier, P. Panchaud, D. Pozzi, E. M. Scanlan, A.-P. Schaffner, and V. Weber, *Pure Appl. Chem.* **79**, 223 (2007).
²S. H. Bauer, *Chem. Rev.* **96**, 1907 (1996).
³C. W. Mathews and K. K. Innes, *J. Mol. Spectrosc.* **15**, 199 (1965).
⁴C. W. Mathews, *J. Mol. Spectrosc.* **19**, 203 (1966).
⁵R. N. Dixon, G. Duxbury, R. C. Mitchell, and J. P. Simons, *Proc. R. Soc. A* **300**, 405 (1967).
⁶M. E. Jacox, *J. Phys. Chem. Ref. Data* **17**, 398 (1988).

- ⁷I. Baraille, C. Larrieu, A. Dargelos, and M. Chaillet, *Chem. Phys.* **282**, 9 (2002).
⁸R. Grimminger, P. M. Sheridan, and D. J. Clouthier, *J. Chem. Phys.* **140**, 164302 (2014).
⁹W. R. M. Graham and W. Weltner, Jr., *J. Chem. Phys.* **65**, 1516 (1976).
¹⁰E. L. Cochran, F. J. Adrian, and V. A. Bowers, *J. Chem. Phys.* **36**, 1938 (1962).
¹¹D. J. Clouthier, *J. Chem. Phys.* **141**, 244309 (2014).
¹²W. W. Harper and D. J. Clouthier, *J. Chem. Phys.* **106**, 9461 (1997).
¹³D. L. Michalopoulos, M. E. Geusic, P. R. R. Langridge-Smith, and R. E. Smalley, *J. Chem. Phys.* **80**, 3556 (1984).
¹⁴E. L. Gamble, H. S. Booth, and H. Halbedel, *Inorganic Syntheses* (Wiley, 1950), Vol. 3.
¹⁵A. D. Becke, *J. Chem. Phys.* **98**, 5648 (1993).
¹⁶C. Lee, W. Yang, and R. G. Parr, *Phys. Rev. B* **37**, 785 (1988).
¹⁷T. H. Dunning, Jr., *J. Chem. Phys.* **90**, 1007 (1989).
¹⁸D. Feller, K. A. Peterson, and J. G. Hill, *J. Chem. Phys.* **135**, 044102 (2011).
¹⁹M. J. Frisch, G. W. Trucks, H. B. Schlegel *et al.*, GAUSSIAN 09, Revision A.02, Gaussian, Inc., Wallingford, CT, 2009.
²⁰D.-S. Yang, M. Z. Zgierski, A. Bérces, P. A. Hackett, P.-N. Roy, A. Martinez, T. Carrington, Jr., D. R. Salahub, R. Fournier, T. Pang, and C. Chen, *J. Chem. Phys.* **105**, 10663 (1996).
²¹E. V. Doktorov, I. A. Malkin, and V. I. Man'ko, *J. Mol. Spectrosc.* **64**, 302 (1977).
²²T. Masiello, A. Maki, and T. A. Blake, *J. Mol. Spectrosc.* **243**, 16 (2007).
²³T. Wentink, Jr. and V. H. Tiensuu, *J. Chem. Phys.* **28**, 826 (1958).
²⁴G. Herzberg, *Molecular Spectra and Molecular Structure III. Electronic Spectra and Electronic Structure of Polyatomic Molecules* (Van Nostrand, New York, 1966).
²⁵P. J. Bruna, M. R. J. Hachey, and F. Grein, *Mol. Phys.* **94**, 917 (1998).
²⁶F. Grein, *J. Phys. Chem A* **102**, 10869 (1998).